Correlation between evolution of resistive switching and oxygen vacancy configuration in $La_{0.5}Ca_{0.5}MnO_3$ based memristive devices

2012 Nanotechnology 23 265202

(http://iopscience.iop.org/0957-4484/23/26/265202)

Nanotechnology **23** (2012) 265202 (7pp) doi:10.1088/0957-4484/23/26/265202

Correlation between evolution of resistive switching and oxygen vacancy configuration in $La_{0.5}Ca_{0.5}MnO_3$ based memristive devices

Zhi-Hong Wang[1,3,4], Yang Yang[1,3], Lin Gu[1,4], H-U Habermeier[2], Ri-Cheng Yu[1], Tong-Yun Zhao[1], Ji-Rong Sun[1] and Bao-Gen Shen[1]

[1] Beijing National Laboratory for Condensed Matter Physics, Institute of Physics, Chinese Academy of Sciences, Beijing 100190, People's Republic of China
[2] Max-Planck-Institute for Solid State Research, Heisenbergstrasse 1, D-70569, Stuttgart, Germany

E-mail: z.wang@iphy.ac.cn and l.gu@iphy.ac.cn

Received 16 February 2012, in final form 17 May 2012
Published 15 June 2012
Online at stacks.iop.org/Nano/23/265202

Abstract
We here report a study of the correlation between the evolution of resistive switching and the oxygen vacancy configuration in $La_{0.5}Ca_{0.5}MnO_3$ (LCMO) based memristive devices. By taking advantage of LCMO located at a phase boundary of the metal-to-insulator transition, we observe the development of the high resistive states, depending upon not only the electrical pulse magnitude but also the switching cycles. We discuss the experimental results by an oxygen migration model that involves both single isolated and clustered oxygen vacancies, which are later verified using aberration-corrected scanning transmission electron microscopy.

The resistive switching phenomenon discovered in metal–oxide–metal structures has attracted intense research interest as it encompasses intriguing physics and the promise of applications in nonvolatile memristive devices [1, 2]. Among the concerted efforts for understanding its physical mechanism, the phenomenological model in terms of oxygen vacancy (ion) electromigration has received much attention [3–14]. On the one hand, this is because the oxygen vacancy is one of the fundamental defects in oxides and its migration driven by current or voltage pulses can occur at ambient and even cryogenic conditions [15, 16]. On the other hand, this can also be attributed to the well-known fact that oxygen vacancies indeed enable critical impacts on the electrical properties for a large variety of compounds. In the past five years, many works have focused on the resistive switching properties (the resistive change ratio, retention, endurance, etc) by tailoring oxygen vacancies via various techniques [7–9, 11–14]. Despite significant progress achieved in the device performance [17], the guidelines for the oxygen vacancy engineering remain elusive, and to date, the knowledge on oxygen vacancies and their migration during the resistive switching is far from adequate.

Here, we report a study of the correlation between the evolution of resistive switching and the oxygen vacancy configuration in $La_{0.5}Ca_{0.5}MnO_3$ (LCMO) based devices. As a typical perovskite manganite in the phase diagram of $La_{1-x}Ca_xMnO_3$, LCMO is best known by its charge–orbital ordering state at low temperatures [18]. In the present work, however, it is chosen for its other prime feature, i.e. this half-doped manganite locates at a phase boundary of the metal ($x < 0.5$) to insulator ($x > 0.5$) transition, and because of this characteristic, we expect that a subtle local development with the oxygen vacancies (configuration and concentration) should bring forth a discernible resistive evolution at the metal–oxide interface.

Epitaxial LCMO films were grown onto (001) $SrTiO_3$ (STO) single crystal substrates (5×5 mm^2) by pulsed laser deposition using a KrF excimer laser with a 5 Hz pulse rate and a 1.6 J cm^{-2} energy density. The films were deposited in

[3] These authors contributed equally to this work.
[4] Authors to whom any correspondence should be addressed.

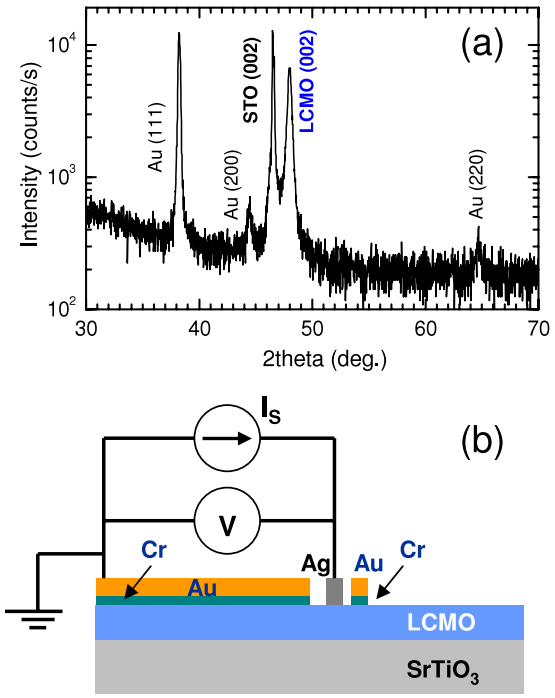

Figure 1. (a) The x-ray diffraction pattern for the LCMO film; (b) a schematic view of the device structures and the two-probe electrical measurements. The arrows indicate the Cr seeding layer (in cyan) between the Au electrode (in orange) and the LCMO film.

a 0.4 mbar oxygen atmosphere at 850 °C and subsequently annealed in a 1 bar oxygen atmosphere at 900 °C for 15 min. The x-ray diffraction pattern (figure 1(a)) confirms a single phase and (00*l*) oriented growth. For the fabrication of a planar device shown in figure 1(b), a Cr/Au pad (Au-P0, ~2.5 × 5 mm^2) with Cr as the seeding layer was deposited onto the half film surface using E-beam evaporation, while a small Ag contact (~0.25 × 0.5 mm^2) was fabricated by printing and curing high quality silver-filled epoxy adhesive (H20E) with ~0.2 mm separation on to the close boundary of the Au-P0 pad. In addition, a small reference Cr/Au electrode (Au-P1, ~0.3 × 0.6 mm^2) was deposited adjacent to the Ag electrode. The various electrical responses were measured at 300 K by the two-probe method. The current pulse was applied to the small electrode with Au-P0 being grounded. To avoid perturbing the interfacial states, the junction resistance was always recorded using a small measuring current of 10 μA.

Figure 2 shows the current–voltage (*I*–*V*) responses to different current maxima (I_{max}) from the device of Ag/LCMO/Au-P0, plotted on a semilog scale (figures 2(a)–(b)) and partially on a linear scale (figures 2(a′)–(b′)). It can be clearly seen that the *I*–*V* curves are non-linear and the hysteresis initially presents with I_{max} = 20 mA and then gets much expanded with I_{max} = 30 mA, indicating an evolution of the resistive switching behavior that occurs between a high resistive (HR) state in negative bias and a low resistive (LR) state in positive bias. For a comparison, the *I*–*V* responses from the reference device of Au-P1/LCMO/Au-P0 were also measured. As illustrated in figures 2(b)–(b′), its *I*–*V* curve shows a linear behavior with little hysteresis even when I_{max} = 30 mA. This fact indicates that (i) the electrical contact between the LCMO film and the

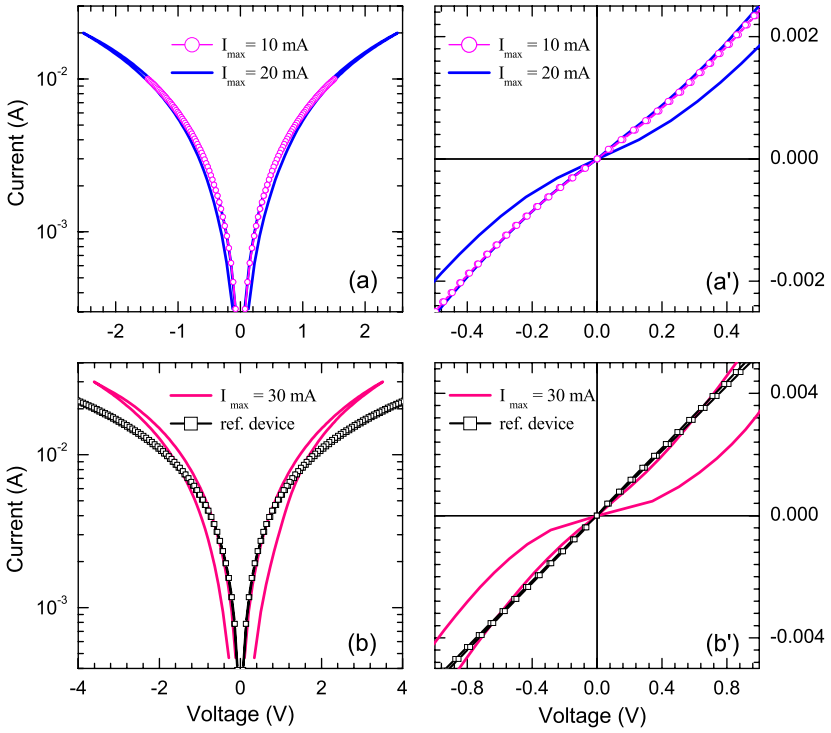

Figure 2. The ambient *I*–*V* responses from the Ag/LCMO/Au-P0 device with different I_{max}, plotted on a semilog scale ((a)–(b)) and a linear scale for the data in the low bias regime ((a′)–(b′)). For a comparison, the *I*–*V* curve for the reference device Au-P1/LCMO/Au-P0 is also shown in (b)–(b′).

Cr/Au electrode is ohmic; (ii) the electroresistance is absent in the reference device; and importantly (iii) the non-ohmic electrical contact between the small Ag electrode and the LCMO film plays a crucial role in the creation of the resistive switching behavior.

To detail the evolution of the resistive switching in Ag/LCMO/Au-P0, the cycle dependence of the resistive switching was carefully measured in the writing–reading–erasing mode using bipolar electrical pulse trains (positive–negative–positive–$\cdots$) with different kinds of magnitudes (I_p = 10, 20, and 30 mA), and in addition to the instant resistive response at ∼0 s, the short-time relaxation (within ∼50 s) was monitored every 10 s after switching off each discrete pulse. As clearly seen in figures 3(a) and (b), only with $I_p \geq 20$ mA can the current pulses give rise to a pronounced resistive switching, which is in good agreement with the I–V measurements. Interestingly, with increasing switching cycles in the case of $I_p = 20$ mA, the HR profile monotonically increases and finally gets nearly saturated. By contrast, the enhanced HR profile in the case of $I_p = 30$ mA is promptly set, and with increasing switching cycles it exhibits no systematic change but some fluctuations as also confirmed by the repeated measurement (figure 3(b)). In all the cases, the LR states appear to be stable at about 250 Ω, however, the HR states exhibit a visible resistive relaxation. The average short-time relaxation rate for the HR states has been assessed by

$$\Delta R/(R\Delta t) = [R(\sim 0\ \mathrm{s}) - R(50\ \mathrm{s})]/[R(\sim 0\ \mathrm{s})\Delta t], \qquad (1)$$

where $\Delta t = 50$ s, and $R(\sim 0$ s) and $R(50$ s) are the initial resistive response driven by the electrical pulsing at ∼0 s and the resistance at 50 s after switching off the current pulse, respectively. Figure 3(c) plots the relaxation rates as a function of the observation time. In a close correlation with the evolution of the HR profile, the relaxation rates with I_p = 20 mA first increase and then become nearly constant with increasing switching cycles. For the two cases of $I_p = 30$ mA, however, the relaxation rates are approximately constant since the very beginning and they are apparently larger than those with $I_p = 20$ mA.

Due to their importance to practical applications, the endurance and retention properties of memristive devices have been extensively explored. But so far, much less attention has been paid to the initial evolution of the resistive switching. In a $Pr_{0.7}Ca_{0.3}MnO_3$ film based device, Odagawa *et al* [19] reported a developing resistive switching behavior similar to the present case of $I_p = 20$ mA. However, they did not provide an explanation of the observed phenomenon. For the present bipolar switching device, the negative (positive) electrical pulses drive the oxygen vacancies into (away from) the Ag–LCMO interface, thus partially breaking (rehabilitating) the Mn–O–Mn chains for electron hopping and in turn increasing (lowering) the device resistance. Note that the trapping centers randomly located near the Ag–LCMO interface could cause a minor difference in the oxygen vacancy distribution between successive electrical pulses. If each time the single negative pulse of the same I_p involves a constant number of mobile oxygen vacancies, the HR profile

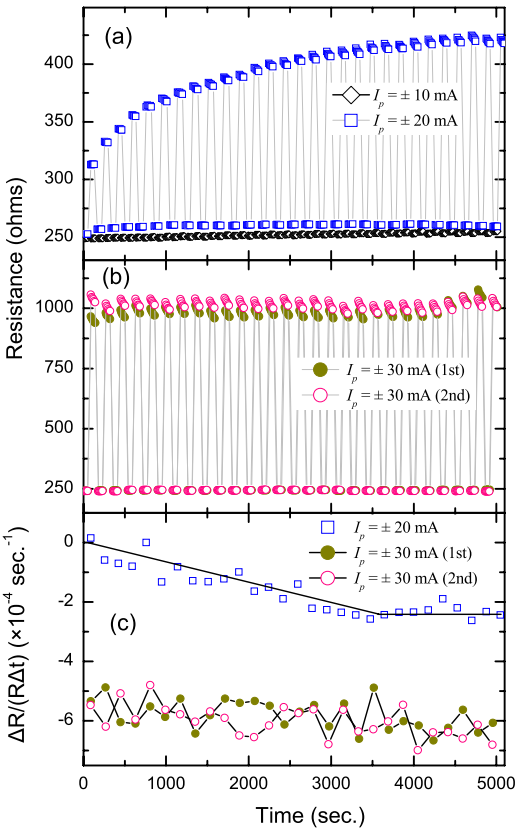

Figure 3. Resistive switching responses from the Ag/LCMO/Au-P0 device measured in the writing–reading–erasing mode using bipolar electrical pulse trains (positive–negative–positive–$\cdots$) with different I_p: (a) I_p = 10 and 20 mA; (b) $I_p = 30$ mA measured for two times. In all the cases, in addition to the instant resistive response driven by the electrical pulsing at ∼0 s, the short-time relaxation (within ∼50 s) was monitored every 10 s after switching off each discrete pulse. Note that there is little resistive switching effect in the case of $I_p = 10$ mA, the resistive responses are almost merged in a line with $R \approx 250$ Ω (shown in open diamonds in (a)). (c) The relaxation rates of the HR states (shown in (a)–(b)) as a function of the observation time. The straight line is a guide for the eyes.

should not show a systematic cycle dependence but just some fluctuations [8], as can be seen in the cases of $I_p = 30$ mA. It thus appears that an enriched concentration of oxygen vacancies should be incorporated with increasing switching cycles in the case of $I_p = 20$ mA. To shed more light on this process, we extract the instantaneous HR response [$R_{\mathrm{ins}} = R(\sim 0$ s)] induced by the negative pulses of $I_p = 20$ mA from figure 3(a), and plot them versus the switching cycle numbers (n) in figure 4. By using the least squares method, we find that the evolution behavior can be well fitted with a double-exponential function (see the solid line in figure 4):

$$R_{\mathrm{ins}}(n) = C_0 + C_1 \exp(-n/P_1) + C_2 \exp(-n/P_2). \qquad (2)$$

Here, the C_i parameters have the dimension of resistance (Ω) while the P_i parameters are dimensionless and resemble a time constant associated with the switching cycle numbers. The P_i parameters obtained from the fit are: $P_1 = 1.26 \pm 0.31$ and $P_2 = 10.42 \pm 0.57$. Such fast and slow responses naturally lead

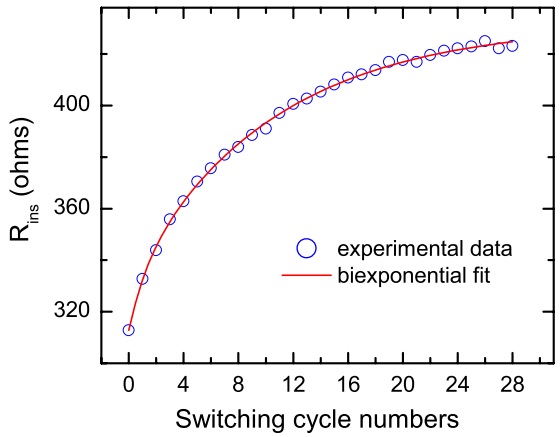

Figure 4. The instantaneous HR response (R_{ins}) versus switching cycle numbers in the case of $I_p = 20$ mA. The line is from a bi-exponential fitting (see the context).

us to conjecture different atomic configurations of oxygen vacancies that may be involved in the resistive switching processes.

In general, oxygen vacancies are known to exist as single isolated point defects [20, 21]. However, for perovskite oxides [22–24] as well as some binary oxides [25–28] that are prone to be oxygen deficient, strong interactions between oxygen vacancies can occur, causing them to cluster or order in correlated form. We note that assuming an existence of oxygen vacancy clustering in the present LCMO films, the experimental results can be consistently interpreted as follows.

First, as indicated by the first-principles calculation performed recently by Cuong *et al* [23], the migration energy barrier for oxygen vacancies in correlated form is larger than that of a single isolated oxygen vacancy. Hence, a negative electrical pulse with I_p up to 20 mA would just induce a swift attraction of single isolated oxygen vacancies towards the Ag–LCMO interface, causing a moderate rise in the device resistance. Second, with the initial motion of single isolated oxygen vacancies, local atomic rearrangements could occur [29], allowing some clustered oxygen vacancies to be separated into single isolated vacancies and/or smaller sized vacancy clusters which can be later driven to the metal–oxide interface by the subsequent electrical pulses. With such kinetic processes of oxygen vacancies in isolated and correlated forms, which are actually revealed by the fast and slow responses in the bi-exponential fit, respectively, the oxygen vacancy concentration should be gradually enriched at the Ag–LCMO interface, which in turn gives rise to the developing HR profile in the case of $I_p = 20$ mA. It also becomes clear that, by applying a stimulus at a higher energy level ($I_p = 30$ mA), more vacancies both in isolated and correlated forms would be promptly driven to the interface, leading to an abrupt establishing of HR profile of an enhanced

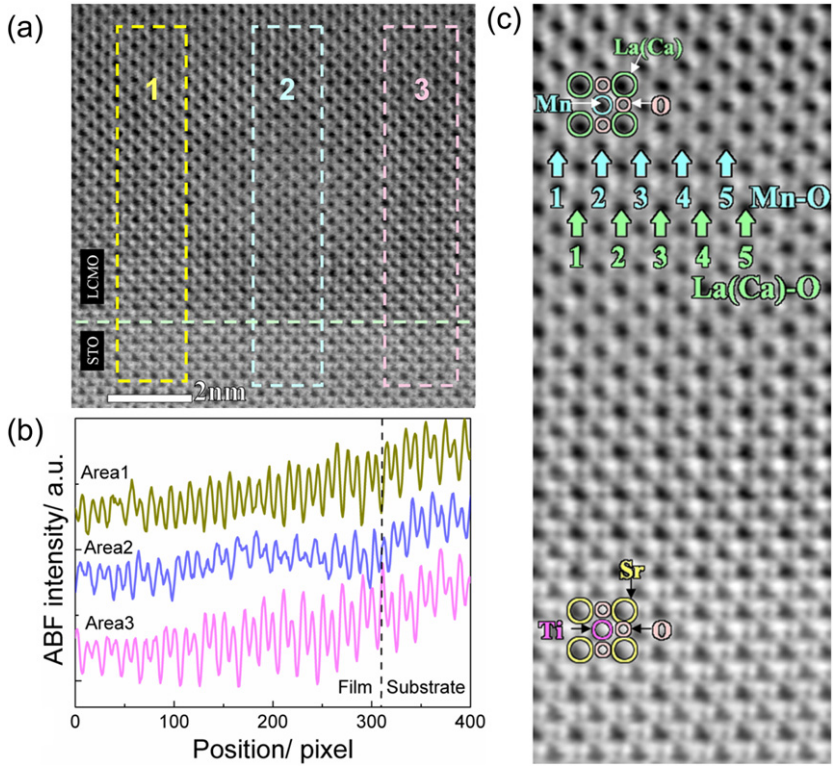

Figure 5. (a) The annular-bright-field (ABF) micrograph taken along the [100] direction in a cross-section specimen of the LCMO film. The dashed line indicates the interface between LCMO and STO; (b) the integral ABF line profiles of the rectangular areas 1–3 shown in (a) along the [001] direction; (c) the enlarged micrograph of the area 2, in which the different atoms and the checked Mn–O and La(Ca)–O chains were labeled by numbers and arrows (see the context).

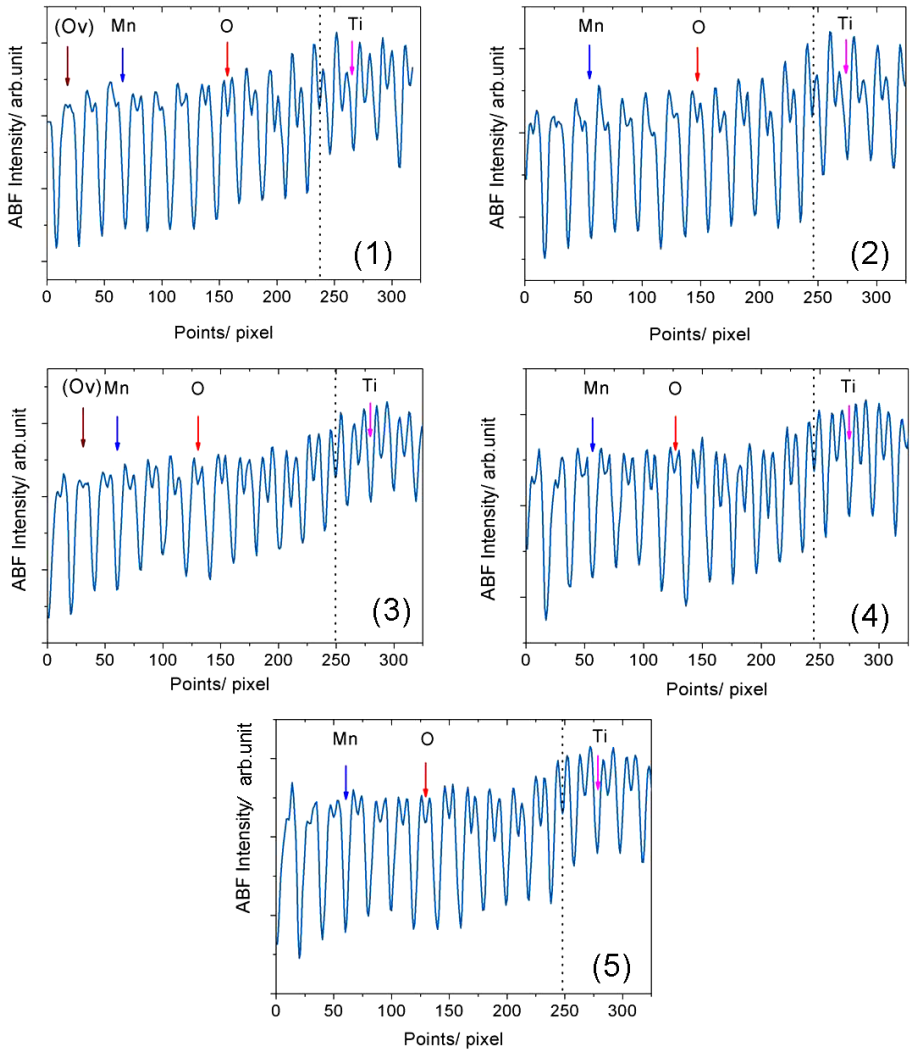

Figure 6. The ABF line profiles (1)–(5) for the corresponding single atom Mn–O chains that are indicated in figure 5(c). Besides cations and oxygen ions, oxygen vacancies (O_v) are indicated by arrows in the weakened wave troughs of the intensity curves. The dashed line indicates the interface between LCMO and STO, labeled according to the intensity change in both the ABF and the corresponding high-angle annular-dark-field images acquired simultaneously in the same area.

resistance. On the other hand, with an enriched concentration of oxygen vacancies at the Ag–LCMO interface, an increased fraction of vacancies would be driven into a nonequilibrium distribution, and the stronger Coulomb repulsive interactions between the oxygen vacancies will accelerate the vacancy diffusion away from the interface [3]. This explains why the resistive relaxation rates are larger in the case of $I_p = 30$ mA; and in the case of $I_p = 20$ mA, the relaxation rates are gradually increased to an approximately constant value with increasing switching cycles.

For a verification of the presence of oxygen vacancy clustering in the LCMO film, we further exploited an aberration-corrected scanning transmission electron microscope (STEM), which can directly image the oxygen atoms with atomic resolution. The STEM observation was carried out on a JEOL 2100F transmission electron microscope (JEOL, Tokyo, Japan) operated at 200 keV. The effective probe size was defined to be ∼0.9 Å at an incident angle of 25 mrad. The cross-sectional specimens for the STEM analysis were carefully thinned down to obtain electron transparency. In particular, the final ion-beam milling was performed on a low energy, low-angle parameter and liquid-nitrogen cooled stage to avoid damage to the film microstructure.

Figure 5(a) shows a typical annular-bright-field (ABF) micrograph taken along the [100] direction in a cross-section specimen of the LCMO film. In this image the cation sites of La(Ca), Mn, Ti and Sr columns are revealed in dark contrast with different intensities, while, in particular, with extended sensitivity for light atoms in the ABF configuration [30], the O sites can be identified as lighter dots between each of the two cations [31]. Clearly, the LCMO film was epitaxially grown on STO with a sharp LCMO–STO interface. However, as far as the lattice coherence is concerned, there exist regions, the marked area 2, for instance, exhibiting different intensity profiles from the surroundings. As preliminarily analyzed in figure 5(b), the integral ABF line profile seen along the [001] direction shows regular and similar patterns for both

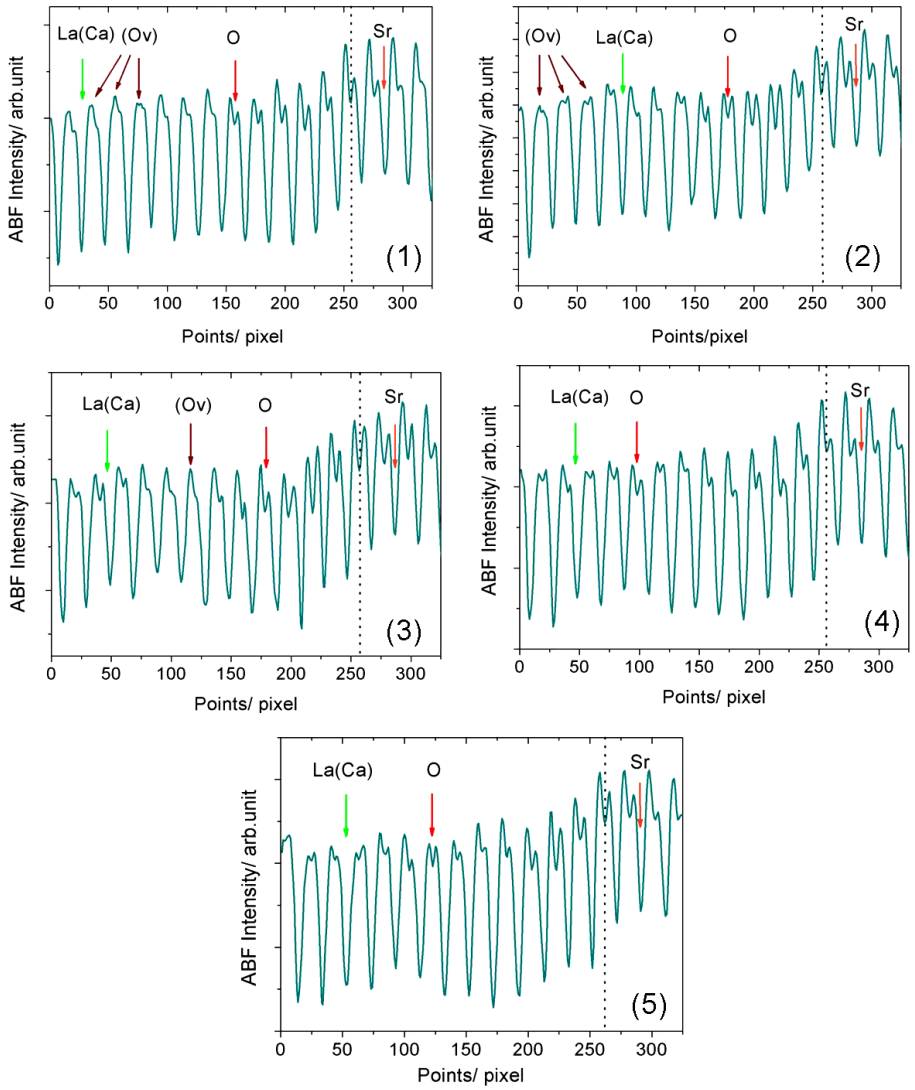

Figure 7. The ABF line profiles (1)–(5) for the corresponding single atom La(Ca)–O chains that are labeled in figure 5(c). Besides cations and oxygen ions, oxygen vacancies (O_v) are indicated by arrows in the weakened wave trough of the intensity curves. The dashed line indicates the interface between LCMO and STO, labeled according to the intensity change in both the ABF and the corresponding high-angle annular-dark-field images acquired simultaneously in the same area.

film and substrate in the adjacent areas 1 and 3; whereas in the area 2 it shows an irregular pattern only for the film, implying the existence of lower atom occupancy in this area. It is worth noting that, to avoid a preferential thinning effect at the dislocation cores during the ion-beam sample preparation [32], the ABF micrograph was taken not including misfit dislocations that were generated by the strain relaxation and were observed elsewhere at the LCMO–STO interface. In such an instance, the detected lower atom occupancy should be attributed to the atomic vacancies inherent to the LCMO film.

Figure 5(c) shows the enlarged micrograph of the area 2. To check the existence of oxygen vacancies in this area, we carefully obtained the ABF line profiles (figures 6 and 7) along the five Mn–O chains and five La(Ca)–O chains indicated by the numbers and arrows in figure 5(c). Note that the intensities in atomic sites of La(Ca), Mn, O are weaker than the surroundings; they are revealed by the different wave troughs denoted by the arrows in the intensity profiles. As characterized by an obvious decrease of depth in some wave troughs corresponding to the O sites, oxygen vacancies in single isolated oxygen columns (figures 6(1) and (3), 7(3)) and also neighboring oxygen columns (figures 7(1) and (2)) can be clearly resolved in Mn–O and La(Ca)–O chains, indicating the presence of oxygen vacancies and vacancy clustering, which thereby supports our model on the evolution of the resistive switching.

In summary, with detailed electrical measurements and aberration-corrected STEM characterization, a resistive switching evolution has been captured in LCMO based devices, and explained by an oxygen migration model that involves not only the single isolated oxygen vacancies but also the oxygen vacancy clustering. To the best of our knowledge, the oxygen vacancy configurations (in single isolated form or in clusters) have so far been rarely clarified in studies on resistive switching. We believe, however, they are crucial for

understanding the physics of resistive switching, and their substantial impact deserves imperative attention in terms of defect engineering in memristive devices.

Acknowledgments

The authors (Z-HW and H-UH) are grateful to G Cristiani, M Schulz and G Gregori at MPI-Stuttgart for their technical assistance. This work was supported by the National Natural Science Foundation of China (Grant Nos 10774173, 1174353 and 10974235), the National Basic Research Program of China and the Beijing Natural Science Foundation.

References

[1] Sawa A 2008 *Mater. Today* **11** 28
[2] Ha S D and Ramanathan S J 2011 *J. Appl. Phys.* **110** 071101
[3] Nian Y B, Strozier J, Wu N J, Chen X and Ignatiev A 2007 *Phys. Rev. Lett.* **98** 146403
[4] Quintero M, Levy P, Leyva A G and Rozenberg M J 2007 *Phys. Rev. Lett.* **98** 116601
[5] Janousch M, Meijer G I, Staub U, Delley B, Karg S F and Andreasson B P 2007 *Adv. Mater.* **19** 2232
[6] Yang J J, Pickett M D, Li X, Ohlberg D A A, Stewart D R and Williams R S 2008 *Nature Nanotechnol.* **3** 429
[7] Shi J P, Zhao Y G, Zhang H J, Tian H F and Zhang X P 2009 *Appl. Phys. Lett.* **94** 192103
[8] Yang M K, Park J-W, Ko T K and Lee J K 2009 *Appl. Phys. Lett.* **95** 042105
[9] Do Y H, Kwak J S, Bae Y C, Jung K, Im H and Hong J P 2009 *Appl. Phys. Lett.* **95** 093507
[10] Rozenberg M J, Sánchez M J, Weht R, Acha C, Gomez-Marlasca F and Levy P 2010 *Phys. Rev.* B **81** 115101
[11] Jeong H Y, Lee J Y and Choi S-Y 2010 *Appl. Phys. Lett.* **97** 042109
[12] Shibuya K, Dittmann R, Ma S and Waser R 2010 *Adv. Mater.* **22** 411
[13] Goux L, Czarnecki P, Chen Y Y, Pantisano L, Wang X P, Degraeve R, Govoreanu B, Jurczak M, Wouters D J and Altimime L 2010 *Appl. Phys. Lett.* **97** 243509
[14] Wang S-Y, Lee D Y, Huang T-Y, Wu J-W and Tseng T-Y 2010 *Nanotechnology* **21** 495201
[15] Scott J F and Dawber M 2000 *Appl. Phys. Lett.* **76** 3801
[16] Yi H T, Choi T and Cheong S-W 2009 *Appl. Phys. Lett.* **95** 063509
[17] Jo S H, Kim K-H and Lu W 2009 *Nano Lett.* **9** 870
[18] Radaelli P G, Cox D E, Marezio M and Cheong S-W 1997 *Phys. Rev.* B **55** 3015
[19] Odagawa A, Sato H, Inoue I H, Akoh H, Kawasaki M, Tokura Y, Kanno T and Adachi H 2004 *Phys. Rev.* B **70** 224403
[20] Tuller H L and Bishop S R 2011 *Annu. Rev. Mater. Res.* **41** 369
[21] Ganduglia-Pirovano M V, Hofmann A and Sauer J 2007 *Surf. Sci. Rep.* **62** 219
[22] Muller D A, Nakagawa N, Ohtomo A, Grazul J L and Hwang H Y 2004 *Nature* **430** 657
[23] Cuong D D, Lee B, Choi K M, Ahn H-S, Han S and Lee J 2007 *Phys. Rev. Lett.* **98** 115503
[24] Loshkareva N N, Mushnikov N V, Korolyov A V, Neifeld E A and Balbashov A M 2008 *Phys. Rev.* B **77** 052406
[25] Nöenberg H and Briggs G A D 1997 *Phys. Rev. Lett.* **79** 4222
[26] Namai Y, Fujui K and Iwasawa Y 2003 *J. Phys. Chem.* B **107** 11666
[27] Zhang C, Michaelides A, King D A and Jenkins S J 2009 *Phys. Rev.* B **79** 075433
[28] Park S, Ahn H-S, Lee C-K, Kim H, Jin H, Lee H-S, Seo S, Yu J and Han S 2008 *Phys. Rev.* B **77** 134103
[29] Ventura J, Araujo J P, Sousa J B, Liu Y, Zhang Z and Freitas P P 2010 *Appl. Phys. Lett.* **96** 043505
[30] Gu L, Zhu C, Li H, Yu Y, Li C, Tsukimoto S, Maier J and Ikuhara Y 2011 *J. Am. Chem. Soc.* **133** 4661
[31] Chisholm M F, Luo W, Oxley M P, Pantelides S T and Lee H N 2010 *Phys. Rev. Lett.* **105** 197602
[32] Jia C L, Thust A and Urban K 2005 *Phys. Rev. Lett.* **95** 225506